# Depth from diffracted rotation

**Adam Greengard**

*Department of Electrical and Computer Engineering, University of Colorado at Boulder, Boulder, Colorado 80309*

**Yoav Y. Schechner**

*Department of Electrical Engineering, Technion—Israel Institute of Technology, Haifa 32000, Israel*

**Rafael Piestun**

*Department of Electrical and Computer Engineering, University of Colorado at Boulder, Boulder, Colorado 80309*

Received August 11, 2005; accepted September 13, 2005

The accuracy of depth estimation based on defocus effects has been essentially limited by the depth of field of the imaging system. We show that depth estimation can be improved significantly relative to classical methods by exploiting three-dimensional diffraction effects. We formulate the problem by using information theory analysis and present, to the best of our knowledge, a new paradigm for depth estimation based on spatially rotating point-spread functions (PSFs). Such PSFs are fundamentally more sensitive to defocus thanks to their first-order axial variation. Our system acquires a frame by using a rotating PSF and jointly processes it with an image acquired by using a standard PSF to recover depth information. Analytical, numerical, and experimental evidence suggest that the approach is suitable for applications such as microscopy and machine vision. 

*OCIS codes:* 110.6880, 110.4850, 100.6640, 150.5670.

The human visual system uses defocus as a depth cue.[1] Optical images convey three-dimensional (3D) information by the amount of blur in each image region: the further the object is from the in-focus plane, the more blurred it appears. This principle is exploited in techniques known as depth from defocus (DFD) by jointly processing frames acquired in different focus or aperture settings.[1–7] Relative to stereovision, DFD is more robust to occlusion and correspondence problems.[8] Moreover, in applications that require a large numerical aperture (NA), particularly in high-magnification microscopy, DFD is more suitable than stereovision.

Previous DFD work has concentrated on the implementation of signal processing algorithms based on a geometrical optical model. Typical systems have utilized a clear, circular aperture as is found in standard camera lenses.[1–7] However, the point-spread function (PSF) of such systems has not been optimized for depth estimation. Therefore in this Letter we engineer the PSF to achieve enhanced performance in this specific task. We exploit the freedom provided by diffractive optics to design unconventional optical responses. In particular, we investigate 3D PSFs whose transverse cross sections rotate with respect to each other as a result of diffraction in free space.[9–14] Rotating PSFs provide a faster rate of change with depth than PSFs of clear pupil systems having the same NA.[9] As a consequence, we show here that rotating PSFs present approximately an order of magnitude increase in Fisher information (FI) along the depth dimension, when compared with standard pupils. Finally, we demonstrate this principle in an experiment based on a two-channel system that encodes a rotating PSF.

The more dissimilar the PSF is at different values of defocus, the easier it is to distinguish between depth planes in the presence of noise. Defocus is typically quantified by the defocus parameter $\psi$, defined as[15]

$$\psi = \frac{2\pi}{\lambda}\left(\frac{1}{z_{\mathrm{obj}}^{\mathrm{focus}}} - \frac{1}{z'_{\mathrm{obj}}}\right) r^2, \tag{1}$$

where $\lambda$ is the wavelength of light, and $z_{\mathrm{obj}}^{\mathrm{focus}}$ and $z'_{\mathrm{obj}}$ are the in-focus and actual object distances from the entrance pupil, respectively. Here $r$ is the radius of the exit pupil that defines the NA of the system.

To quantitatively compare PSFs we evaluate the FI (Ref. 16) with respect to defocus. The reason we choose this criterion is that it indicates the potential accuracy of the depth estimate. Following Ref. 16, the reciprocal of the FI is the Cramer–Rao bound, which is the lower bound of the variance over all unbiased estimators of the parameter. In our case, the FI is calculated with respect to defocus, hence a higher FI value implies a potential for a more accurate estimation of the defocus parameter, and thus the depth of the object.

In our problem the FI per pixel $j$ is evaluated as

$$J_j(\psi) = \sum_h p_j[h(\psi)]\left\{\frac{d}{d\psi}\log p_j[h(\psi)]\right\}^2, \tag{2}$$

where $p_j[h(\psi)]$ is the probability density function of the normalized intensity $h(\psi)$, at pixel $j$, of the PSF with defocus $\psi$. This probability density function depends on the noise statistics and the variation of the expected intensity of the PSF. We evaluate the Fisher information of the entire PSF with respect to defocus as $J(\psi) = \Sigma_j J_j(\psi)$. In our subsequent example we emulate noise as a white Gaussian process with zero mean.

We now show that the FI with respect to defocus can be significantly increased by use of a rotating PSF. The transverse intensity distributions of a ro-

0146-9592/06/020181-3/$15.00 

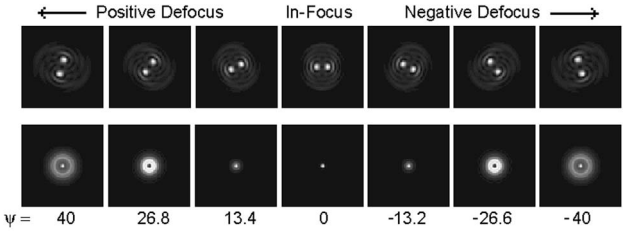


Fig. 1. Intensity of a rotating point-spread function (PSF) (above) and a standard PSF (below) of the same numerical aperture as they go through focus. Note that the standard PSF is essentially constant around focus, while the rotating PSF changes substantially.

tating PSF continuously scale and rotate relative to each other through defocus, as seen, for example, in Fig. 1. Rotating PSFs are inherently different before and after focus. As shown in Ref. 9, the rate of rotation with defocus is linear to first-order approximation. For coherent light, such distributions are formed by a particular combination of Gauss–Laguerre modes and can be optically encoded in phase or amplitude masks.[9] For instance, the PSF shown in Fig. 1 is a superposition of modes with indices $(m,n)$ equal to (1,1), (3,5), (5,9), (7,13), and (9,17), where the indices are defined in Ref. 9. This PSF is designed to produce a rotation of almost $\pi$ within our range of interest ($-40<\psi<40$). Beyond this range the PSF continues to rotate while expanding.

We work with spatially incoherent quasi-monochromatic illumination. Hence the incoherent PSF is the squared modulus of the coherent PSF described above. Figure 1 compares the rotating PSF with a standard PSF that results from a clear, circular pupil of the same NA. The standard PSF hardly varies near focus because there are only second-order changes to the PSF scale. This is in contrast to the first-order changes in the rotating PSF (Ref. 9).

Figure 2 shows the normalized FI with respect to defocus of the rotating PSF and the standard PSF for different values of the defocus parameter. For this calculation we assume independent, additive white Gaussian noise in each PSF cross section. The PSFs are both normalized such that their maximum intensity is equal to one; the variance of the noise is 0.0001. The rotating PSF clearly has higher FI around the in-focus depth plane. In addition, the FI is nearly constant across the depth range of interest for the rotating PSF, whereas the standard PSF varies greatly, dipping to zero at the in-focus plane. This means that with a rotating PSF it is possible to estimate depth across a wide range, instead of arbitrarily favoring some depth planes over others, as the standard PSF does. The null FI of the standard PSF at the focal plane indicates insensitivity to defocus at that plane. This is the result of its almost constant transverse profile (see Fig. 1). The gain in depth discrimination of rotating PSFs stems partially from their extended cross section. An extended area includes more resolution elements and hence more degrees of freedom for axial changes.

We now describe a method that exploits these principles. For a general object, the detected image, $i_{\mathrm{rot}}$, is proportional to the convolution of the object intensity distribution $i$ and the depth-dependent transverse PSF, $h_{\mathrm{rot}}(\psi)$. The first step in estimating depth is to recover this transverse PSF by use of two frames and a deconvolution algorithm. Two images are needed to make the DFD estimation well posed.[1–7,14,17] Hence in addition to $i_{\mathrm{rot}}$, we acquire a reference frame, $i_{\mathrm{ref}}$. We prefer a reference that is the least sensitive to defocus while being relatively sharp throughout the range of interest. In the following example we acquire the reference frame by stopping down the aperture of the standard system to half that of the rotating PSF system. The two frames can be acquired in parallel or sequentially.

The rotating PSF $h_{\mathrm{rot}}$ is naively estimated by deconvolution as

$$\hat{h}_{\mathrm{rot}}(\psi)=\mathbf{F}^{-1}\{H_{\mathrm{rot}}(\psi)\}=\mathbf{F}^{-1}\left\{\frac{I_{\mathrm{rot}}}{I_{\mathrm{ref}}}H_{\mathrm{ref}}\right\}=\mathbf{F}^{-1}\left\{\frac{IH_{\mathrm{rot}}(\psi)}{IH_{\mathrm{ref}}}H_{\mathrm{ref}}\right\},\tag{3}$$

where $\mathbf{F}$ denotes Fourier transform while $I=\mathbf{F}i$, $I_{\mathrm{rot}}=\mathbf{F}i_{\mathrm{rot}}$, and $I_{\mathrm{ref}}=\mathbf{F}i_{\mathrm{ref}}$. $H_{\mathrm{rot}}$ and $H_{\mathrm{ref}}$ are the optical transfer functions of the rotating and the reference PSFs, respectively. Both $H_{\mathrm{rot}}$ and $H_{\mathrm{ref}}$ can be precomputed or calibrated.

Because deconvolution is ill conditioned, it requires regularization. In our experiments, we regularize the solution by computing

$$\hat{h}_{\mathrm{rot}}(\psi)=\mathbf{F}^{-1}\left\{\frac{I_{\mathrm{ref}}^{*}}{|I_{\mathrm{ref}}|^{2}+\sigma^{2}}I_{\mathrm{rot}}H_{\mathrm{ref}}\right\}\tag{4}$$

instead of Eq. (3), where $\sigma$ is a regularization parameter and * denotes the complex conjugate.

As an example we demonstrate this process with a 4-$f$ demagnifying imaging system, with focal lengths 500 and 250 mm. The NA of the entrance pupil is 0.011. The rotating PSF is realized with a computer-generated hologram placed in the Fourier plane. The illumination source is a He–Ne laser at 633 nm, expanded to a spot size of ~10 mm. A rotating diffuser phase modulates the beam to make the light effectively spatially incoherent. The test object is a U.S.

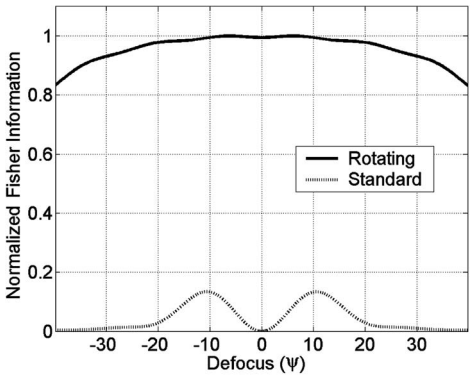


Fig. 2. Normalized FI of the rotating and standard PSFs as they go through focus. The rotating PSF clearly has higher and more constant FI.

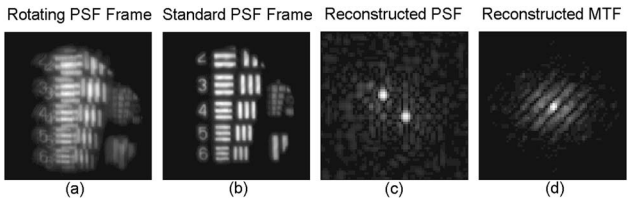


Fig. 3. Frames obtained with (a) rotating PSF and (b) standard PSF. Reconstructed transverse (c) PSF and (d) MTF.

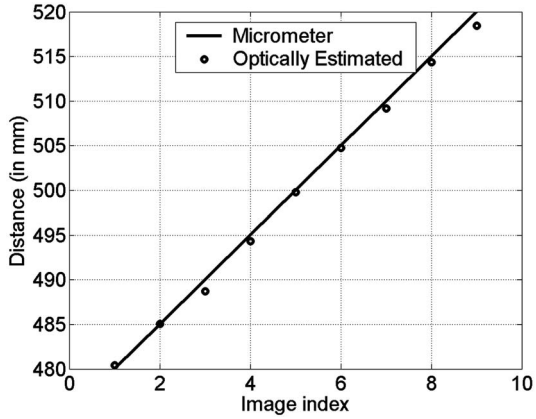


Fig. 4. Estimated (circles) and actual depths (line) of the resolution chart test object. The average absolute error is 0.66 mm, or 1.6% of the entire depth range. For comparison, the depth of field of a classical optical system of the same dimensions is 5.3 mm.

Air Force resolution chart. Figure 3 shows sample frames. The frame corresponding to the rotating PSF looks essentially like a superposition of an image with its translated version. The direction and distance of this translation encode the depth information. The rotating PSF derived by deconvolution is shown in Fig. 3 in conjunction with its corresponding modulation transfer function (MTF). The recovered PSF closely resembles a calibrated PSF at the depth of the target.

Once the PSF is recovered, we estimate depth by measuring the angle of rotation of the transverse PSF. We may also estimate the spot size of this PSF, as is done with traditional depth from defocus. Following Ref. 9, the estimated depth $\hat{z}$ is related to the angle of rotation as

$$\hat{z}'_{\mathrm{obj}} = \left( \frac{z_0 \tan\frac{\phi}{2}}{z_{\mathrm{img}}^2} + \frac{1}{z_{\mathrm{obj}}^{\mathrm{focus}}} \right)^{-1}, \qquad (5)$$

where $z_0$ is the Rayleigh range of the basic Gauss–Laguerre beam that generates the PSF,[9] $\phi$ is the angle of rotation, and $z_{\mathrm{img}}$ is the distance to the in-focus image plane. In practice, a more accurate relation between the depth and the rotation angle is achieved by calibrating the system. As seen in Fig. 3, the deconvolved transverse PSF has two distinct maxima that indicate the rotation angle. We thus estimate the depth by recovering the PSF, measuring its orientation $\phi$, and then using the calibration curve that relates rotation to depth.

In our demonstration, frames were taken every 5 mm over a 40 mm range. We estimated the angle $\phi$ by the orientation defined by the two maxima of the retrieved rotating PSF. The maxima locations were automatically determined by fitting the spots to two cubic spline functions. The results of the depth estimation are shown in Fig. 4. The average absolute error over the nine frames was 0.66 mm. For reference we note that the object depth of field of the system is $\lambda/\mathrm{NA}^2 \approx 5.3$ mm. Therefore we obtain depth discrimination well below the depth-of-field limit.

In this example the object was normal to the optical axis. In general, however, the object has a three-dimensional structure. The method can be extended to deal with such cases, e.g., by processing the image in blocks, as is customary in DFD literature. A report of these results is being prepared.

In conclusion, we have demonstrated a new depth-imaging paradigm that uses a spatially rotating PSF. Fisher information analysis shows an inherent and significant improvement in depth estimation. We have shown a method to extract depth information from this new PSF as well as experimental results that demonstrate the principle.

This work was supported by the National Science Foundation under grant ECS- 0225533. Y. Y. Schechner is a Landau Fellow, supported by the Taub Foundation, and an Alon Fellow. R. Piestun's e-mail address is rafael.piestun@colorado.edu.

**References**

1. A. P. Pentland, IEEE Trans. Pattern Anal. Mach. Intell. **9**, 523 (1987).
2. J. Ens and P. Lawrence, IEEE Trans. Pattern Anal. Mach. Intell. **15**, 97 (1993).
3. M. Subbarao and Y. Liu, in Proc. SPIE **3204**, 24 (1997).
4. P. Favaro and S. Soatto, IEEE Trans. Pattern Anal. Mach. Intell. **27**, 406 (2005).
5. A. N. Rajagopalan, S. Chaudhuri, and R. Chellappa, J. Opt. Soc. Am. A **17**, 1722 (2000).
6. D. Rajan and S. Chaudhuri, IEEE Trans. Pattern Anal. Mach. Intell. **25**, 1102 (2003).
7. M. Watanabe and S. K. Nayar, Int. J. Comput. Vis. **27**, 203 (1998).
8. Y. Y. Schechner and N. Kiryati, Int. J. Comput. Vis. **39**, 141 (2000).
9. R. Piestun, Y. Y. Schechner, and J. Shamir, J. Opt. Soc. Am. A **17**, 294 (2000).
10. Y. Y. Schechner, R. Piestun, and S. Shamir, Phys. Rev. E **54**, R50 (1996).
11. R. Piestun and J. Shamir, J. Opt. Soc. Am. A **15**, 3039 (1998).
12. P. Paakkonen, J. Lautanen, M. Honkanen, M. Kuittinen, J. Turunen, S. N. Khonina, V. V. Kotlyar, V. A. Soifer, and A. T. Friberg, J. Mod. Opt. **45**, 2355 (1998).
13. J. Courtial, K. Dholakia, D. A. Robertson, L. Allen, and M. J. Padgett, Phys. Rev. Lett. **80**, 3217 (1998).
14. A. Greengard, Y. Y. Schechner, and R. Piestun, in Proc. SPIE **5557**, 91 (2004).
15. J. W. Goodman, *Introduction to Fourier Optics*, 2nd ed. (McGraw-Hill, 1996), Chap. 5.
16. T. M. Cover and J. A. Thomas, *Elements of Information Theory* (Wiley-Interscience, 1991).
17. E. R. Dowski and W. T. Cathey, Appl. Opt. **33**, 6762 (1994).